Acta Crystallographica Section D
Biological Crystallography
ISSN 0907-4449

Active-site models for complexes of quinolinate synthase with substrates and intermediates

Erika V. Soriano, Yang Zhang, Keri L. Colabroy, Jennie M. Sanders, Ethan C. Settembre, Pieter C. Dorrestein, Tadhg P. Begley and Steven E. Ealick*

Department of Chemistry and Chemical Biology, Cornell University, Ithaca, NY 14853-1301, USA

Correspondence e-mail: see3@cornell.edu

Received 21 December 2012
Accepted 7 May 2013

PDB Reference: quinolinate synthase, 4hhe

Quinolinate synthase (QS) catalyzes the condensation of iminoaspartate and dihydroxyacetone phosphate to form quinolinate, the universal precursor for the *de novo* biosynthesis of nicotinamide adenine dinucleotide. QS has been difficult to characterize owing either to instability or lack of activity when it is overexpressed and purified. Here, the structure of QS from *Pyrococcus furiosus* has been determined at 2.8 Å resolution. The structure is a homodimer consisting of three domains per protomer. Each domain shows the same topology with a four-stranded parallel β-sheet flanked by four α-helices, suggesting that the domains are the result of gene triplication. Biochemical studies of QS indicate that the enzyme requires a [4Fe–4S] cluster, which is lacking in this crystal structure, for full activity. The organization of domains in the protomer is distinctly different from that of a monomeric structure of QS from *P. horikoshii* [Sakuraba *et al.* (2005), *J. Biol. Chem.* **280**, 26645–26648]. The domain arrangement in *P. furiosus* QS may be related to protection of cysteine side chains, which are required to chelate the [4Fe–4S] cluster, prior to cluster assembly.

1. Introduction

Nicotinamide adenine dinucleotide (NAD) is an essential redox cofactor in various metabolic pathways, where it serves as a hydride acceptor or donor. Recently, NAD has been discovered to play nonredox roles in several signaling pathways, including aging, calcium-dependent signaling and DNA repair, leading to a renewed interest in NAD biosynthesis, as reviewed in Berger *et al.* (2004), Knight & Milner (2012) and Pollak *et al.* (2007). In addition, NAD has been shown to serve as a substrate in the biosynthesis of thiamin phosphate (Chatterjee *et al.*, 2007). In the *de novo* biosynthesis of NAD, quinolinate is the universal precursor for the pyridine ring (Begley *et al.*, 2001).

Quinolinate is synthesized differently in eukaryotes and prokaryotes (Fig. 1). In eukaryotes, the biosynthetic pathway requires five enzymes to convert tryptophan to quinolinate (Begley *et al.*, 2001; Kurnasov *et al.*, 2003; Magni *et al.*, 1999). In contrast to the tryptophan pathway, most prokaryotes utilize a much simpler pathway to synthesize quinolinate which requires only two enzymes (Begley *et al.*, 2001; Magni *et al.*, 1999). The first enzyme, L-aspartate oxidase (LASPO), oxidizes aspartate to the unstable intermediate iminoaspartate (Nasu *et al.*, 1982). This enzyme has been well characterized in several organisms and has been found to utilize oxygen or succinate as the oxidizing source under aerobic or anaerobic conditions, respectively (Seifert *et al.*, 1990; Flachmann *et al.*, 1988; Bacchella *et al.*, 1999). The second enzyme, quinolinate synthase (QS), is encoded by the *nadA* gene and catalyzes

the condensation reaction of iminoaspartate and dihydroxyacetone phosphate (DHAP) to form quinolinate (Suzuki *et al.*, 1973; Nasu & Gholson, 1981).

An iron–sulfur cluster was predicted for *Escherichia coli* QS (EcQS) based on the motif CX_2CX_2C (Sun & Setlow, 1993; Gardner & Fridovich, 1991; Draczynska-Lusiak & Brown, 1992). A [4Fe–4S] cluster that is required for activity was subsequently confirmed for the *E. coli* enzyme (Cicchillo *et al.*, 2005; Ollagnier-de Choudens *et al.*, 2005). Yet many QSs lack the conserved CX_2CX_2C motif observed in EcQS, including the QSs from *Arabidopsis thaliana*, *Bacillus subtilis*, *Mycobacterium tuberculosis* and *Pyrococcus horikoshii*, amongst others. Although these organisms lack the conserved motif, studies have shown that they still require a [4Fe–4S] cluster as a common cofactor (Loiseau *et al.*, 2005; Narayana Murthy *et al.*, 2007; Marinoni *et al.*, 2008; Saunders *et al.*, 2008).

Two mechanisms have been proposed for QS (Begley *et al.*, 2001; Sakuraba *et al.*, 2005). While they differ in some of their details, they both predict 5-hydroxy-4,5-dihydroquinolinate as the final intermediate. Experimental characterization of QS has been challenging because of its tendency to form inclusion bodies and its oxygen-sensitivity (Ceciliani *et al.*, 2000). Thus, mechanistic evidence is based mostly on labeling studies using partially purified *E. coli* QS (Wicks *et al.*, 1977). The structure of *P. horikoshii* QS (PhQS) with a bound substrate analog has been reported (PDB entry 1wzu; Sakuraba *et al.*, 2005). The crystal structure revealed a novel fold and a striking domain similarity, suggesting that the domains were the result of gene triplication. The structure lacked a [4Fe–4S] cluster. The authors did not mention the requirement for an iron–sulfur cluster or identify any possible cysteine residues involved in cluster formation.

QS from *P. furiosus* (PfQS) is a 34 kDa protein with 303 amino acids. It is 84% identical to PhQS and 34% identical to EcQS. PfQS also lacks the [4Fe–4S] cluster motif that is found in the *E. coli* enzyme. PfQS overexpresses in substantial quantities, thus providing an advantage for structural and mechanistic studies. Here, we report the crystal structure of PfQS at 2.8 Å resolution. In contrast to the monomeric PhQS, PfQS exists as a dimer in the crystal structure. While the first

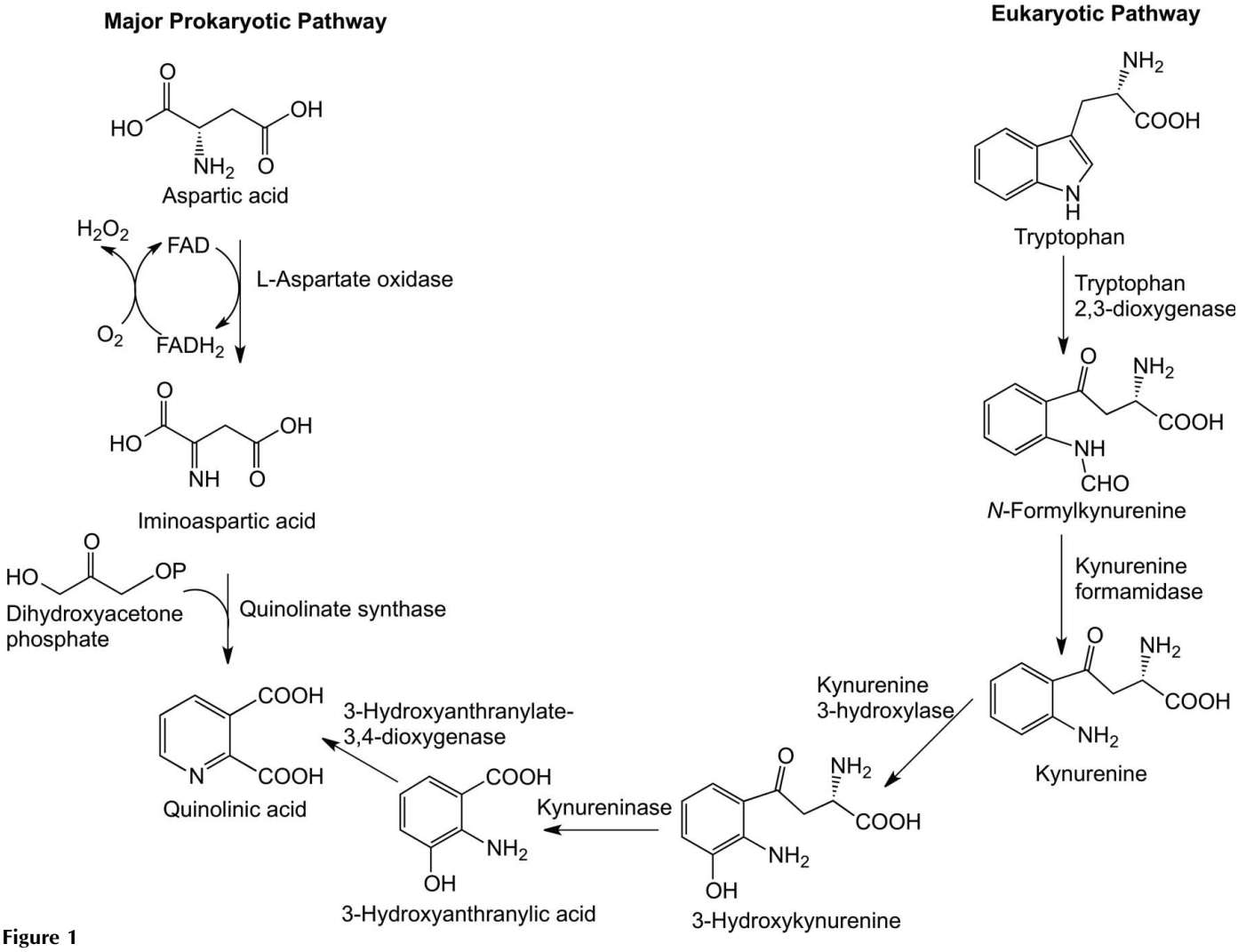

Figure 1
Two pathways for quinolinate biosynthesis. On the left is the pathway found in most prokaryotes, in which quinolinate derives from aspartate and dihydroxyacetone phosphate. On the right is the pathway found in most eukaryotes, in which quinolinate derives from tryptophan.

two domains of PfQS and PhQS superimpose well, the third domain is repositioned by a rotation of about 180° and a translation of approximately 25 Å compared with PhQS. As expressed in *E. coli*, PfQS shows no detectable activity; however, following reconstitution with iron and sulfide a specific activity of 0.033 µmol min^{-1} mg^{-1} was observed. We used the structures of PfQS and PhQS and the similarity of the individual domains to IspH (Gräwert *et al.*, 2010) and Dph2 (Zhang *et al.*, 2010), two enzymes containing [4Fe–4S] clusters, to construct a model of the QS enzyme–substrate complex.

2. Experimental procedures

2.1. Molecular cloning

Standard methods were used for DNA manipulations (Ausubel & Brent, 1987; Sambrook *et al.*, 1989). Plasmid DNA was purified with a Qiagen Miniprep kit and DNA fragments were purified from agarose gel with a Nucleospin Purification kit (Macherey-Nagel). *E. coli* strain MachI (Invitrogen) was used as a recipient for transformations during plasmid construction and for plasmid propagation and storage.

The PfQS gene (*nadA*) was PCR-amplified from genomic DNA (ATCC 43587D) using the primer pair 5′-TAG TAG **CAT ATG** GAA AAG GTT GAG GAG CTT AAG AAG-3′ (inserts an *Nde*I site at the start codon) and 5′-TAG TAG **CTC GAG** TCA ACT CAT CTC AAG CAT TCT TTC-3′ (inserts an *Xho*I site after the stop codon). The amplified DNA was cloned into plasmid pSTBlue-1 using a Perfectly Blunt cloning kit (Novagen). A representative clone sequence was verified and the *nadA* gene was excised by digestion with *Nde*I and *Xho*I. The gene was ligated into similarly digested pET-28a (Novagen) to give plasmid pPfNadA.28 and into pET-16b (Novagen) to give plasmid pPfNadA.16. PfQS was crystallized using pPfNadA.28, while pPfNadA.16 was used for the biochemical studies.

2.2. Protein expression and purification

The pPfNadA.16 or pPfNadA.28 construct containing the N-terminally polyhistidine-tagged *nadA* gene was transformed into the *E. coli* overexpression strain BL21(DE3) (Novagen). Native protein was obtained by inoculating 1 l LB and 40 µg ml^{-1} kanamycin with 5 ml of a saturated starter culture. The cells were then grown at 310 K until they reached an OD_{600} of ∼0.6, at which point the cells were induced with 500 µ*M* isopropyl *β*-D-1-thiogalactopyranoside. After 4 h induction, the cells were spun down at 5000*g* for 10 min and stored at 193 K.

For production of the selenomethionine-incorporated (SeMet) protein, the methionine-auxotrophic strain of *E. coli*, B834(DE3) (Novagen), was transformed with the above plasmid and the cells were grown using slightly different growth conditions to those described above. The 1 l growth medium contained M9 salts supplemented with 40 µg ml^{-1} of all amino acids except L-methionine, which was replaced by L-selenomethionine, 0.4%(*w*/*v*) glucose, 2 m*M* $MgSO_4$, 25 µg ml^{-1} $FeSO_4{\cdot}7H_2O$, 0.1 m*M* $CaCl_2$, 40 µg ml^{-1} kanamycin, 1 m*M* dithiothreitol (DTT) and 1% BME vitamin solution (Gibco-BRL). The cells from the initial 5 ml starter culture were also washed with the above medium and used to start a 50 ml culture. This second culture was grown to an OD_{600} of ∼0.6 and was used to inoculate a larger 1 l culture. The rest of the expression was performed as described above.

All purification steps were carried out at 277 K. All buffers contained 1 m*M* DTT for the SeMet-incorporated protein. The cells were resuspended in 20 ml lysis buffer (50 m*M* NaH_2PO_4, 300 m*M* NaCl, 10 m*M* imidazole pH 8.0) and were lysed using a French press. The crude extract was centrifuged and the resulting supernatant was mixed for 1 h with 500 µl of Ni–NTA beads (Novagen) equilibrated with lysis buffer. The beads were then added to a polypropylene column and washed with 200 ml lysis buffer. The column was first eluted with 50 ml of wash buffer containing 20 m*M* imidazole to remove weakly binding proteins. PfQS was eluted from the column using elution buffer containing 250 m*M* imidazole. After gel filtration using an Econo-Pac 10DG column (Bio-Rad) and elution with 25 m*M* Tris pH 7.6, the protein was concentrated to 25 mg ml^{-1} using a 10 kDa cutoff concentrator (Amicon) and stored at 193 K. A light brown color was observed in some of the purified protein batches. Protein concentration was determined by the Bradford method using bovine serum albumin as the standard (Bradford, 1976). The purity of QS was determined by Coomassie-stained SDS–PAGE analysis and was found to be 95–99% (data not shown).

2.3. Crystallization

Both native and SeMet PfQS were crystallized using the hanging-drop vapor-diffusion method at 295 K with drops consisting of 2 µl protein solution and 1 µl well solution. The protein concentration was 25 mg ml^{-1} and the well solution for optimized conditions consisted of 4.3–4.5 *M* NaCl, 50 m*M* Tris pH 7.3–7.9, 4–6% ethylene glycol. Crystals appeared within two weeks and grew to their maximum size (0.8 × 0.4 × 0.2 mm) in four weeks. The crystallization conditions for the SeMet protein were the same as described above except that 1 m*M* DTT was added to the protein solution. Crystals were cooled by plunging them directly into liquid nitrogen without any additional cryoprotectant and stored. Initial X-ray data showed that both the SeMet and the native crystals belonged to space group *I*222. The SeMet crystals had unit-cell parameters $a = 77.1$, $b = 80.8$, $c = 141.4$ Å. The unit-cell parameters for the native crystals were $a = 76.9$, $b = 80.7$, $c = 141.0$ Å. All data sets contained one protomer per asymmetric unit, corresponding to a solvent content of 61% and a Matthews coefficient of 3.2 $Å^3$ Da^{-1} (Matthews, 1968).

2.4. X-ray data collection and processing

X-ray diffraction data were collected on beamline 8-BM at the Advanced Photon Source (APS) using a Quantum 315 detector (Area Detector Systems Corporation). A single-wavelength anomalous diffraction data set was collected at the selenium peak. To minimize the effects of crystal decay, Bijvoet pairs were measured using inverse-beam geometry in

Table 1
Summary of data-collection and processing statistics for PfQS.

Values in parentheses are for the highest resolution bin.

	SeMet, peak	Native
Wavelength (Å)	0.9791	0.9795
Resolution (Å)	2.7	2.8
Space group	*I*222	*I*222
Unit-cell parameters (Å)		
a	77.1	76.9
b	80.8	80.7
c	141.4	141.0
No. of reflections	136269	98697
No. of unique reflections	12468	11147
Multiplicity	10.9 (9.3)	8.9 (9.1)
Completeness (%)	98.5 (97.8)	99.7 (100)
$R_{\rm merge}$† (%)	11.1 (41.5)	10.5 (40.5)
$\langle I/\sigma(I)\rangle$	22.4 (3.6)	22.5 (6.6)

† $R_{\rm merge} = \sum_{hkl}\sum_i |I_i(hkl) - \langle I(hkl)\rangle|/\sum_{hkl}\sum_i I_i(hkl)$, where $\langle I(hkl)\rangle$ is the mean intensity of the *i* reflections with intensity $I_i(hkl)$ and common indices *hkl*.

two 90° passes with an oscillation range of 1.0°. Crystals of native PfQS were difficult to grow, were highly mosaic and decayed rapidly even under cryogenic cooling. While the $\langle I/\sigma(I)\rangle$ value at the highest resolution was 6.6, the $R_{\rm merge}$ was 40% and it was our judgement that the data beyond 2.8 Å resolution contributed little to the quality of the maps or the refinement. Because of the rapid decay of the crystals, two native data sets were collected at a wavelength of 0.9791 Å and scaled together. The *HKL*-2000 suite (Otwinowski & Minor, 1997) was used to index, integrate and scale all data sets. Table 1 summarizes the final data-collection and processing statistics.

2.5. Structure determination

The direct-methods program *SnB* (Miller *et al.*, 1993, 1994) was used to locate the positions of the Se atoms. *SnB* gave eight of the 11 possible Se sites. Anomalous difference Fourier maps and log-likelihood Fourier maps calculated in *CNS* (Brünger *et al.*, 1998) were used to find the additional three sites and to improve the initial phases. The Se atom of Met92 showed a minor site; however, only the major site was used for phase calculation. The phases were recalculated and density modification was used to further improve the initial phases.

2.6. Model building and refinement

Model building was performed using the computer programs *O* (Jones *et al.*, 1991) and *Coot* (Emsley & Cowtan, 2004). Protein masks and bones representations of the electron density from the program *MAPMAN* (Kleywegt & Jones, 1996) were used to build a polyalanine model. Domains 1 and 2 had strong electron density and were built first; however, owing to the poor quality of the maps in the region of domain 3 most of this domain was not incorporated into the initial model. Refinement using the SeMet PfQS data set and *REFMAC* (Murshudov *et al.*, 2011), with TLS restraints, along with several rounds of rigid-body, annealing and *B*-factor refinement in *CNS* improved the map, and most of the side chains for domains 1 and 2 were built. At this point the model was refined against the native data. Domain 3 was built using domains 1 and 2 as a guide based on the evidence of gene triplication. After several rounds of refinement the side chains of domain 3 were added, with three Met residues matching the three sites that were located by *SnB*. Rounds of refinement were performed using *PHENIX* (Adams *et al.*, 2002), resulting in a final *R* factor and $R_{\rm free}$ for PfQS of 20.8 and 27.0%, respectively. Final refinement statistics are shown in Table 2.

Table 2
Summary of refinement statistics for PfQS.

Resolution (Å)	50–2.8
Total No. of non-H atoms	2274
No. of protein atoms	2272
No. of Cl^- ions	2
No. of reflections in refinement	11117
No. of reflections in test set	531
R factor† (%)	20.8
$R_{\rm free}$‡ (%)	27.0
Average *B* factors (Å^2)	
Protein main chain	38.6
Protein side chain	39.8
Cl^- ions	32.6
R.m.s. deviations from ideal geometry	
Bonds (Å)	0.005
Angles (°)	0.847
Ramachandran plot	
Most favored regions (%)	90.3
Additional allowed regions (%)	9.7
Disallowed regions (%)	0.0

† *R* factor = $\sum_{hkl}\big||F_{\rm obs}| - |F_{\rm calc}|\big|/\sum_{hkl}|F_{\rm obs}|$, where $F_{\rm obs}$ and $F_{\rm calc}$ are the observed and calculated structure factors, respectively. ‡ For $R_{\rm free}$ the sum is extended over a subset of reflections (10%) excluded from all stages of refinement.

2.7. Reconstitution of the [4Fe–4S] cluster

All of the reconstitution steps were performed under argon and on ice. Purified concentrated PfQS was degassed by blowing argon over the surface of the protein solution while stirring on ice. The protein solution was degassed in an argon-purged 15 ml Nalgene tube and argon was introduced through two holes made in the cap of the tube. After 30 min, a 50-fold stoichiometric excess of DTT was added as a 50 µl solution in degassed 25 m*M* Tris pH 7.6 buffer and the solution was allowed to stir under argon for 10 min. Next, a 50 µl solution of $FeCl_3$ in degassed 25 m*M* Tris pH 7.6 was added in an eightfold stoichiometric excess to PfQS. The solution of $FeCl_3$ was made immediately before addition to PfQS, and it was added *via* syringe under a flow of argon. Finally, a 50 µl solution of an eightfold excess of Na_2S was made in degassed 25 m*M* Tris pH 7.6 and added 5–10 µl at a time over 10 min. Addition was made by syringe under a flow of argon. After addition of the reconstituting agents was complete, an argon flow was maintained over the surface of the solution for 10 min and the tube was then capped tightly and allowed to stir on ice for 1 h. Following the incubation, the reconstitution mixture was centrifuged (clinical centrifuge) at 277 K for 1 h. The dark brown solution was then transferred by syringe under argon to a degassed Econo-Pac 10DG gel-filtration column. The column had previously been made anaerobic by passing 100 ml degassed 25 m*M* Tris pH 7.6 buffer through the column using positive argon pressure. The protein solution

was loaded onto the column and eluted using degassed 25 m*M* Tris pH 7.6 buffer, all under positive argon pressure. The dark green–brown PfQS eluting from the gel-filtration column was collected in argon-purged tubes.

2.8. Identification of PfQS reaction product by HPLC analysis

DHAP (12 µmol) was added to a solution of 500 µl PfQS (335 µ*M*) and 500 µl degassed 25 m*M* Tris pH 7.6 buffer. Iminoaspartate was made from a solution of oxalacetic acid (190 µmol) and ammonia (50 µl, 8.5 *M*) in 250 µl 200 m*M* phosphate buffer pH 5. To start the reaction, 24 µl of the iminoaspartate solution was added to the mixture of PfQS, DHAP and buffer. To determine the effects of added reducing agents, identical reactions were prepared in which one or ten equivalents of sodium dithionite were added. The following control reactions were prepared: DHAP and iminoaspartate with and without sodium dithionite and PfQS with and

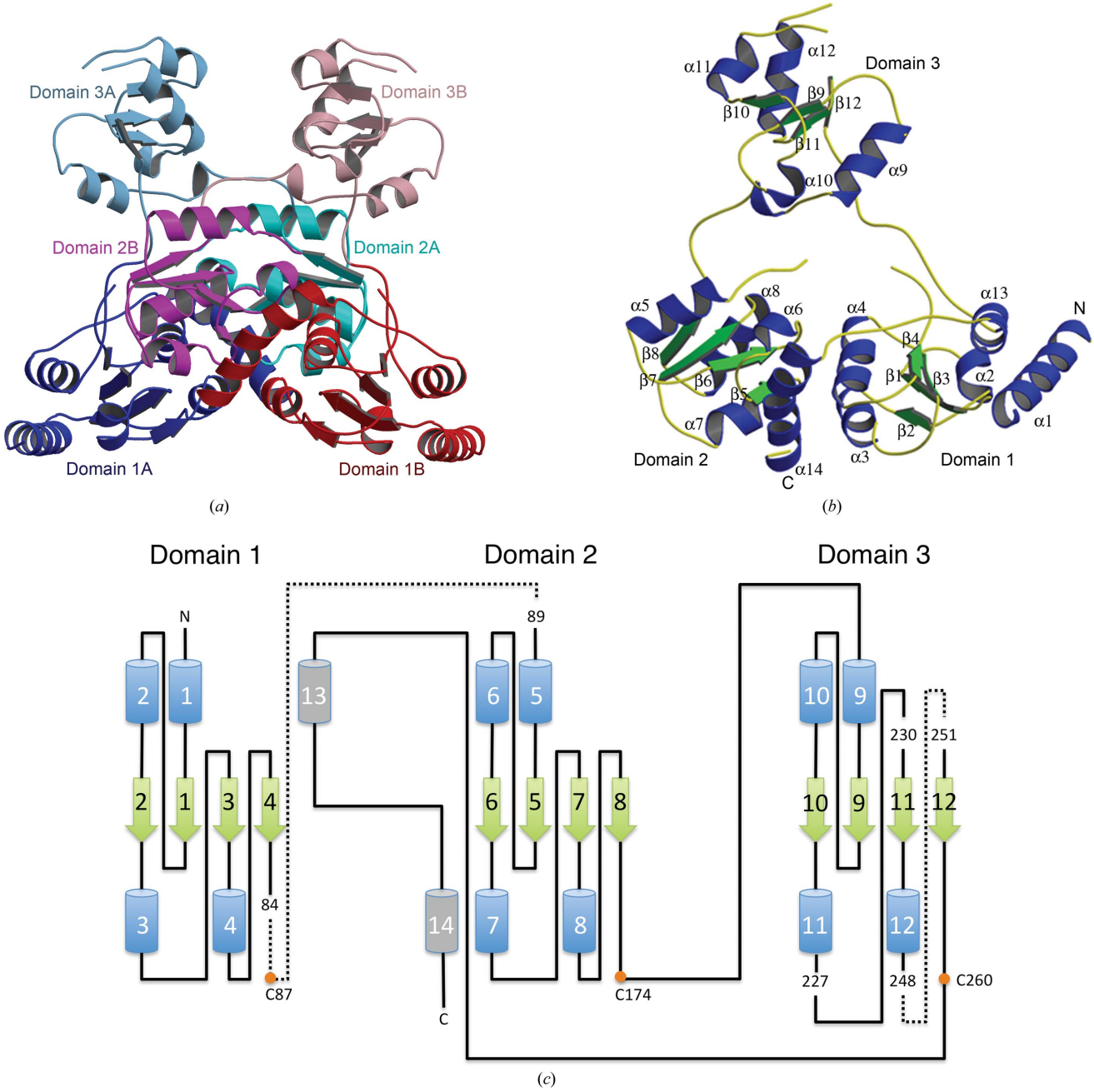

Figure 2
Structure of PfQS. (*a*) Ribbon diagram of the PfQS dimer. Each protomer is colored by domain. The *A* protomer is shown with domain 1 colored in blue, domain 2 in cyan and domain 3 in light blue. The twofold-related *B* protomer is shown with domain 1 in red, domain 2 in magenta and domain 3 in light pink. (*b*) Ribbon diagram for the protomer of PfQS color-coded by secondary structure. The α-helices are shown in blue and the β-strands are shown in green. (*c*) Topology diagram for PfQS. The helices and strands are numbered as in (*b*). Two missing loops are shown as dotted lines with the first and last residues numbered. The three conserved cysteine residues are shown as yellow dots with the corresponding residue number given.

without sodium dithionite. The reactions were tightly capped and incubated for 23 h at room temperature or 328 K. Over time, the initial dark green–brown color of the solutions lightened; the color faded more significantly for the reactions without sodium dithionite. After 23 h, the reaction mixtures were filtered through a membrane (molecular-weight cutoff 10 000) to remove the enzyme. 100 µl of the resulting protein-free reaction mixtures were analyzed by HPLC (Aminex Fast Acid Analysis column, 100 × 7.8 mm, 0.65 ml min^{-1}; solvent *A*, 1.0 m*M* sulfuric acid; solvent *B*, acetonitrile; isocractic, 70% *A*:30% *B*).

2.9. Determination of the specific activity of PfQS

PfQS was purified and its [4Fe–4S] cluster reconstituted as described above. The activity-assay mixture included 10 m*M* dithionite, 0.2 mg reconstituted PfQS, 75 m*M* iminoaspartate (prepared from oxaloacetic acid and ammonia), 5 m*M* DHAP, 50 m*M* Tris pH 7.5, 50 m*M* NaCl. All buffers were extensively degassed and purged with argon before use and all manipulations were performed under positive argon pressure. The reactions were carried out at 328 K, initiated by the addition of iminoaspartate and quenched with 2 *N* H_2SO_4. Because the half-life of iminoaspartate is short (2.5 min at pH 8.0), the reaction was quenched after 5 min to ensure that the enzyme was under saturating conditions. The quenched reactions were filtered using Microcon centrifuge filters and the samples were analyzed by HPLC. The specific activity measured was 0.033 µmol min^{-1} mg^{-1}.

2.10. Figure preparation

All figures were prepared using *MolScript* (Esnouf, 1997, 1999), *Raster3D* (Merritt & Bacon, 1997), *PyMOL* (DeLano, 2002) and *ChemDraw* (CambridgeSoft).

3. Results

3.1. Overall structure

The structure of PfQS was determined to 2.8 Å resolution using single-wavelength anomalous diffraction data. The final model (Fig. 2) contains 297 of 303 amino-acid residues, with residues 85–88 and 249–250 being disordered. Two large residual peaks were modeled as chloride ions. The structure consists of three domains, each containing a short four-stranded parallel β-sheet flanked by four α-helices forming a three-layer $\alpha\beta\alpha$ sandwich. Residues 85–88 are located in a flexible linker between domains 1 and 2, while residues 249–250 are located in a loop region of domain 3. In domain 1, the strand order is 2–1–3–4, with α1, α2 and α13 flanking one side of the β-sheet and α3 and α4 flanking the other and with all

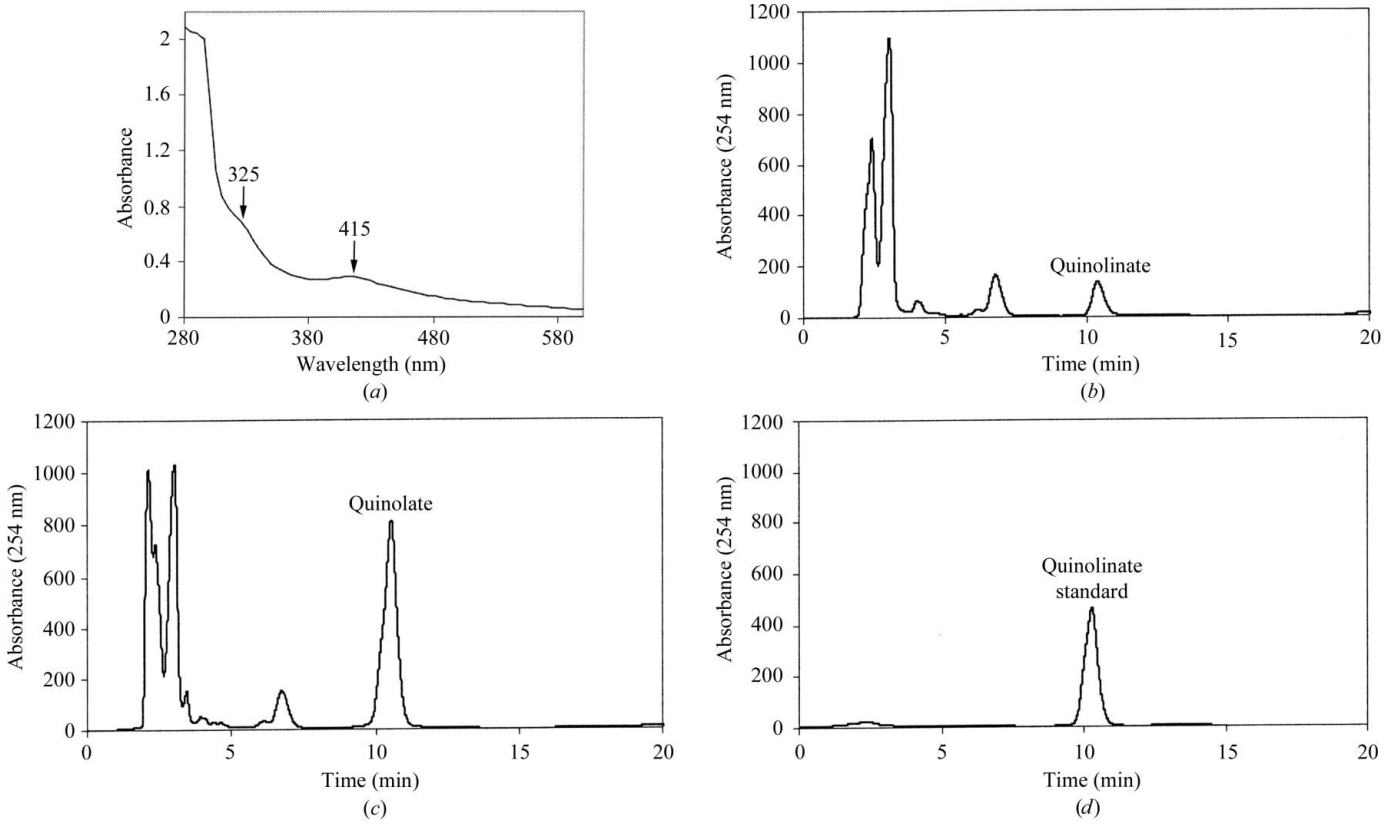

Figure 3
(*a*) UV spectrum showing the characteristic absorbance seen in [4Fe–4S] clusters. (*b*) Production of quinolinate by PfQS. The reaction mixture contained DHAP, iminoaspartate and one equivalent of sodium dithionite. The product quinolinate elutes at 10.5 min. (*c*) Effect of increasing the reducing-agent concentration. The conditions are the same as in (*b*) except that ten equivalents of sodium dithionite were added. (*d*) Quinolinate standard eluting at 10.3 min. Peaks eluting before 10 min were not identified. No quinolinate was detected in the absence of PfQS.

helices running antiparallel to the central β-sheet. Domain 2 has a strand order of 6–5–7–8 for the central β-sheet, which is flanked by α5 and α6 on one side and α7, α8 and α14 on the other, with all helices running antiparallel to the β-sheet. Domain 3 has a strand order of 10–9–11–12, with α9 and α10 flanking one side of the β-sheet and α11 and α12 flanking the other. These helices also run antiparallel to the central β-sheet. The only differences in the topologies of the three domains are the addition of helices α13 and α14 in domains 1 and 2, respectively. The three domains are connected by long flexible linkers, with approximate lengths of 24, 17 and 27 Å for domain 1 to 2, domain 2 to 3 and domain 3 to the C-terminal region, respectively. Each of these linkers contains a cysteine residue that is conserved among all QS proteins. Electron density for domain 3 was weak and the average *B*-factor was 72.3 Å^2, compared with 27.5 and 22.5 Å^2 for domains 1 and 2, respectively.

3.2. Dimeric structure

Two monomers of PfQS form a dimer using twofold crystallographic symmetry (Fig. 2*a*). The approximate dimensions of the dimer are 50 × 65 × 60 Å. The dimer interface is formed by domain 2, the connection between domains 2 and 3 and the connection between domain 3 and the C-terminal α-helices. This unusual dimer formation leaves domain 3 mostly exposed to the solvent and may account for the weak density observed for this domain. The dimer interface buries about 2100 Å^2 of surface area per monomer. There are a total of 12 hydrogen bonds between the two monomers and 13 hydrophobic interactions.

3.3. Biochemical evidence for a [4Fe–4S] cluster

The unreconstituted PfQS used for crystallography was found to be biochemically inactive; however, during the purification some light brown color was noted. PfQS reconstituted under argon showed a dark green–brown color. The UV spectrum of the native PfQS shown in Fig. 3(*a*) contains features at 325 and 415 nm which are consistent with the presence of a [4Fe–4S] cluster.

To test whether the reconstituted enzyme was active, DHAP and iminoaspartate were added to PfQS both with and without sodium dithionite (Figs. 3*b*–3*d*). HPLC analysis of both reactions demonstrated the formation of quinolinate; however, a larger amount of quinolinate was produced in the presence of sodium dithionite (to 20 turnovers). No quinolinate was detected in the absence of PfQS.

4. Discussion

4.1. Possible gene triplication

The structure of PfQS shows three domains with nearly identical topology, suggesting gene triplication. A similar observation was reported for the structure of PhQS (Sakuraba *et al.*, 2005). Multiple sequence alignments using *ClustalW* (Thompson *et al.*, 1994) showed 10% identity and 38% similarity for all three domains. Pairwise comparison of the domains showed 24% identity and 60% similarity for domains 1 and 2, 26% identity and 58% similarity for domains 1 and 3, and 17% identity and 61% similarity for domains 2 and 3. The alignment of all three domains (Fig. 4) showed that the conserved residues are located near the beginning or end of a secondary-structural element, with the exception of the three cysteine residues, which are all located on the flexible linkers.

4.2. Putative active site

Conserved residues were identified from sequence comparisons of QS from different organisms. These residues tend to cluster in a cleft between domains 1 and 2 or on a small patch of domain 3 (Fig. 5*a*). Further evidence for this cleft as the location of the active site is provided by the structure of PhQS, in which the substrate analog malate is found in the same cleft (Sakuraba *et al.*, 2005). Prominent residues in the putative active site of PfQS are His25, Tyr27, Asp41, Ser42, Phe64 and Met65 from domain 1, and Tyr113, Asn115, Lys121, Thr129, Ser130 and Asp150 from domain 2. The dimer of PfQS also contributes residues Tyr113*, Ser130*, Asn152* and Tyr156* to the active-site pocket, where the asterisk indicates residues from a twofold-related monomer. Of the residues from the twofold-related monomer, only Tyr113 is conserved. These residues appear to form a lid over the putative active site, shielding the substrates and products from the solvent. A strong peak in the $F_o - F_c$ electron-density map was found in this region. The residues surrounding the density are hydrophilic on one side and hydrophobic on the other side.

A comparison of the PfQS dimer and the PhQS monomer shows some interesting differences. The putative active site of the dimer forms a much larger pocket because domain 3 is separated from domains 1 and 2 when compared with the monomeric PhQS structure. In the PhQS monomer, the arrangement of domains places conserved residues from all three domains in close proximity, suggesting that the monomer contains a complete active site while the dimer contains a partial active site (Fig. 5*b*). However, it is interesting to note that the PhQS active site does not appear to be large enough for both substrates (Sakuraba *et al.*, 2005).

4.3. [4Fe–4S] cluster

The purified protein was a light brown color, but once the enzyme had been reconstituted with the [4Fe–4S] cluster it was a dark green–brown color. Our biochemical studies confirm that the [4Fe–4S] cluster of PfQS is needed for catalysis. Additionally, the effect of dithionite on the activity of the protein suggests that it may be sensitive to oxygen, another common feature of [4Fe–4S]-containing proteins. While PfQS was inactive before reconstitution of the iron cluster, reconstituted PfQS has a specific activity of 0.033 µmol min^{-1} mg^{-1}. This is comparable to the value for EcQS, the QSs from *A. thaliana*, *B. subtilis* and *M. tuberculosis* and PkQS, all of which required Fe–S cluster reconstitution for activity (Cicchillo *et al.*, 2005; Loiseau *et al.*, 2005; Narayana Murthy *et al.*, 2007; Marinoni *et al.*, 2008; Saunders *et al.*, 2008). All three specific activity values are about 100-fold lower than the value

of 2.2 µmol min^{-1} mg^{-1} reported for PhQS by Sakuraba and coworkers, which did not require reconstitution of an Fe–S cluster.

While PfQS appears to require a [4Fe–4S] cluster, the PfQS sequence does not contain the conserved motif observed in the EcQS sequence (CX_2CX_2C); however, it does contain the last cysteine in the motif (Cys260) and two other conserved cysteine residues, Cys87 and Cys174, all three of which are conserved among all QSs. Mutation of these three conserved cysteine residues in EcQS has been shown to abolish QS activity; thus, these three residues were predicted to be responsible for the formation of the iron–sulfur cluster (Saunders & Booker, 2008; Saunders *et al.*, 2008). However, the first two cysteine residues in the CX_2CX_2C motif are not conserved but have been shown to regulate the activity of the *E. coli* enzyme (Rousset *et al.*, 2008). Each of these three conserved cysteine residues is located on one of the flexible linkers that connect pairs of domains. Cys87 is located in the linker between domains 1 and 2 and is disordered. Cys174 is located in the linker between domains 2 and 3, while Cys260 is located in the linker between domain 3 and the C-terminus. The distance between the Cys174 and Cys260 S atoms is 18 Å; however, when domain 3 is repositioned to superimpose with PhQS the two cysteine residues are much closer together and also near the predicted position of Cys87. The fourth sulfur of the [4Fe–4S] cluster could come from sulfide, although His177, which is located near Cys174 and conserved among all QSs, could also participate in [4Fe–4S] cluster formation. Because all three conserved cysteine residues are disordered in the PhQS structure, their role in the formation of a [4Fe–4S] cluster could not be inferred.

```
PfQS-domain1      1 -MEKVEELKKEIERLKKERNAIILAHNYQLPEVQDVADFVGDSLELARKA  49
PfQS-domain2     88 AMANMLKVKHILEAKKKYPNAPVVLYVNSTAETKAYADVTVTSANAVDII 137
PfQS-domain3    175 YVHKKFTIEDVERAKKLHPNAKLMVHPECNPEVQEHADIIVSTGGMIRRA 224
                     : :   ::.  .  *   ** :: :    .*.:  **.   :

PfQS-domain1     50 TKVDADVIVFAGVDFMAETAKILNPDKIVLIPNKRATC              87
PfQS-domain2    138 RKLDSDVIIFGPDKNLAHYVAKVTGKTIIPIP-PEGHC             174
PfQS-domain3    225 CEWD-EWVVFTEREMVYRLSKLYPNKKFYPAK-EDAVCVGM         263
                     : * : ::*   . : .       ..:       . *
```

Figure 4
Sequence alignment of domains 1, 2 and 3 of PfQS. Identical residues are shown in red font and designated by an asterisk. Conserved residues are designated by a colon or a period. The cysteine residues that provide ligands for the [4Fe–4S] cluster are highlighted in yellow.

4.4. Comparison of PfQS and PhQS

When the entire PfQS model was submitted to *DALI* (Holm & Sander, 1993), the top *Z*-score was 5.8 and corresponded to a D-ribose-binding protein (PDB entry 2dri; Björkman *et al.*, 1994). This protein belongs to the periplasmic binding protein group I superfamily and has a fold that consists of a six-stranded parallel β-sheet with

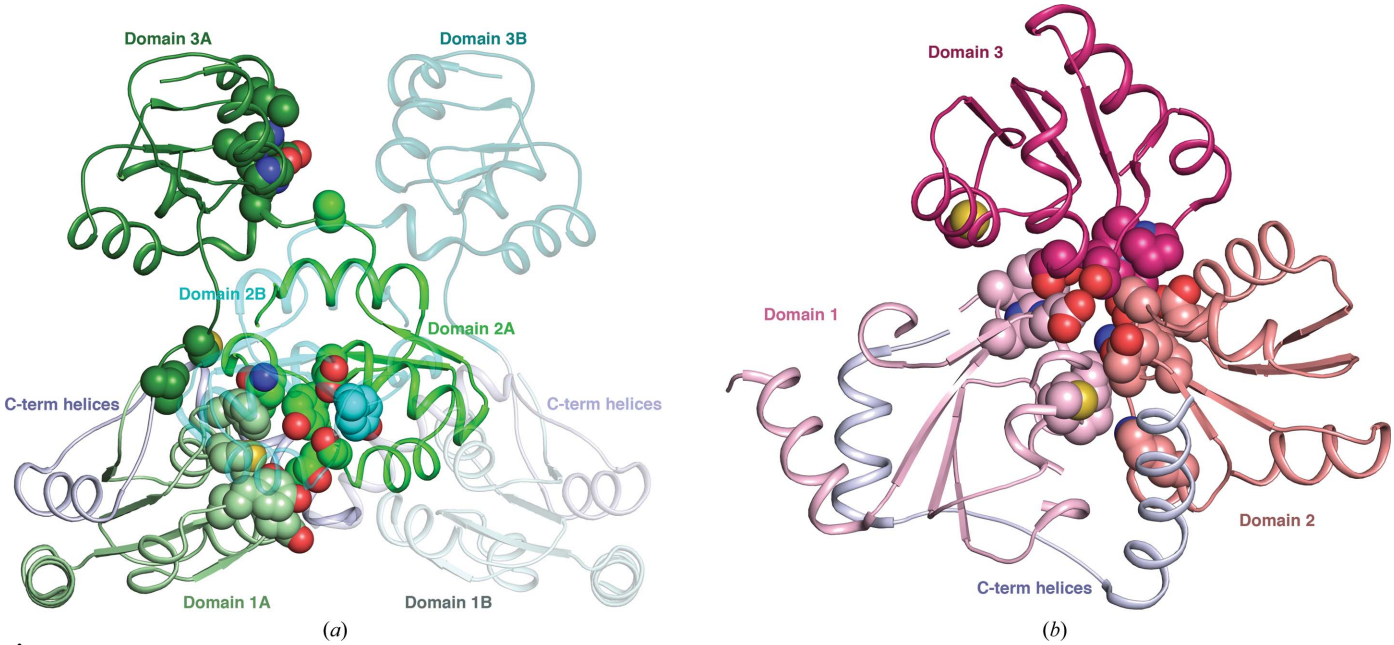

Figure 5
Location of key conserved residues in QS. (*a*) Dimeric structure of PfQS. PfQS is shown as a thin ribbon diagram and the conserved residues are shown as spheres. Domains 1, 2 and 3 are shown in light green, green and dark green for protomer *A* and light blue, cyan and dark cyan for protomer *B*, which is half transparent for clarity of the figure. The two additional helices at the C-terminus are colored light gray for both protomers. The C atoms are color-coded to match the domain color, whereas N, O and S atoms are colored blue, red and yellow, respectively. The conserved residues include His25, Tyr27, Asp41, Ser42, Phe64 and Met65 from domain 1, Tyr113, Asn115, Lys121, Thr129, Ser130, Asp150 and Cys174 from domain 2 and His177, His200, Glu202, Ser216, Thr217, Cys260 and Met263 from domain 3 of one protomer and Tyr113* of the adjacent protomer. (*b*) Conserved residues in the PhQS monomer. PhQS is colored pink, salmon, dark pink and gray for domains 1, 2 and 3 and the C-terminal helices, respectively. The conserved residues are shown as spheres, with C atoms color-coded to match the domain color and other atoms color-coded as in (*a*).

strand order 2–1–3–4–5–6, which is similar to the PfQS structure, which contains the strand order 2–1–3–4. This was surprising because PfQS and PhQS showed 84% identity and 95% similarity. However, when only domain 2 was submitted to the *DALI* server, PhQS appeared as the top hit with a *Z*-score of 15.2 for 92 residues (PDB entry 1wzu; Sakuraba *et al.*, 2005). A *DALI* pairwise comparison between PfQS and PhQS resulted in a higher *Z*-score of 24.0. This discrepancy may result from the difference in oligomeric state and in the relative position of domain 3.

Further structural superposition showed that while the overall domain topologies are the same, only domains 1 and 2 from each structure superimposed well, with an r.m.s.d. of 1.0 Å for 185 residues (Fig. 6). In contrast, domain 3 of PfQS was rotated 176° and translated 26 Å away from domain 3 of PhQS. Both PfQS and PhQS are missing the linker between domains 1 and 2. The PhQS structure also lacks the residues for the linkers between domains 2 and 3 (residues 165–175) and between domain 3 and the C-terminal helices (residues 257–260) (Sakuraba *et al.*, 2005). In contrast, despite the lower resolution for PfQS, the linkers between domains 2 and 3 and between domain 3 and the C-terminal α-helices show clear electron density.

After eliminating the possibility of incorrectly connected domains for both structures, we attempted to model the conformational change that would reposition domain 3 of PhQS onto that of PfQS. The position of domain 3 in PhQS overlaps with the dimer interface of PfQS, suggesting that a dimer cannot form when domain 3 adopts the conformation observed in the PhQS structure. Conversely, the monomer cannot fold without dissociation of the dimer. When the conserved residues are highlighted (Fig. 5*a*), the putative active site is formed in a cleft between domains 1 and 2. The repositioning of domain 3 that is seen in the PhQS structure brings the conserved region in domain 3 near to the putative active site, suggesting that the active form of QS is the monomer (Fig. 5*b*).

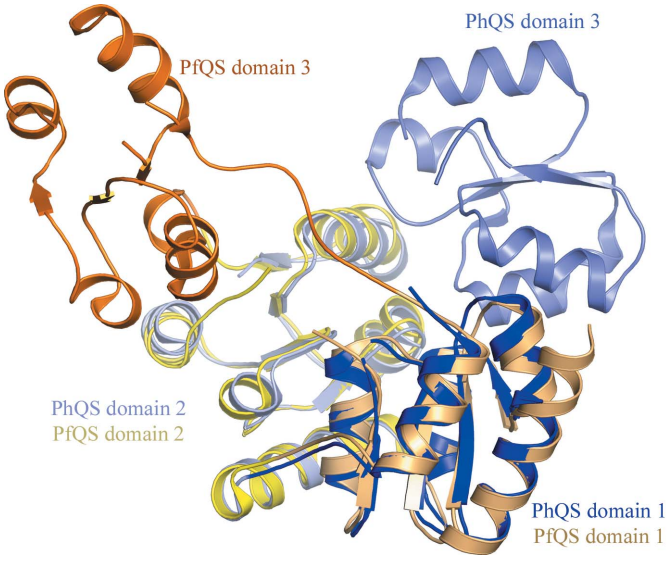

Figure 6
Comparison of the PfQS dimer and the PhQS monomer. Color-coding is by domain as indicated by the labels. Domains 1 and 2 of PfQS and PhQS were used for the superposition.

Attempts to determine the oligomeric state of PfQS in solution using analytical ultracentrifugation, dynamic light scattering and native gel analysis gave inconsistent results. FPLC purification revealed a mixture of monomers and dimers in solution (data not shown). While the dimeric structure of PfQS may be an artifact of crystallization, other possibilities exist. *P. furiosus* is an anaerobic thermophile, therefore it is possible that the linkers provide a hinge that allows domain 3 to reposition under conditions that result in the loss of the [4Fe–4S] cluster or prior to cluster formation. The dimer would allow the protein to remain soluble by covering a hydrophobic patch in the cleft of the putative active site until the [4Fe–4S] cluster could be repaired. In *A. thaliana*, the QS enzyme is fused to a gene implicated in [4Fe–4S] cluster assembly (Loiseau *et al.*, 2005; Narayana Murthy *et al.*, 2007), suggesting the possibility of a complex between PfQS, perhaps in a dimeric state, and a protein required for [4Fe–4S] cluster formation.

In the *de novo* NAD-biosynthesis pathway, the first step of the pathway is the conversion of aspartate to iminoaspartate by LASPO (Nasu *et al.*, 1982). QS then converts iminoaspartate and DHAP to quinolinic acid (Fig. 1; Suzuki *et al.*, 1973; Nasu & Gholson, 1981). Studies using *E. coli* LASPO have shown that iminoaspartate has a half life of 2.5 min at 298 K and pH 8.0 (Nasu & Gholson, 1981), suggesting the possibility of a QS–LASPO complex. Although iminoaspartate is unstable, dialysis experiments that separated *E. coli* LASPO from EcQS still produced the product of the two enzymatic reactions (Wicks *et al.*, 1978). Nevertheless, it is possible that the oligomeric state of QS is related to the formation of the transient QS–LASPO complex or has some other regulatory function.

4.5. Comparison of PfQS, IspH and Dph2

Structural homology searches using *DALI* starting with the complete PfQS monomer failed to show significant similarity to any known structure. A search starting with domain 2 revealed homology to PhQS, but no other significant similarity to known structures. A survey of the literature, however, revealed two proteins, IspH and Dph2, that have three-domain structures in which the domains are structurally homologous to those of PfQS and PhQS. IspH (PDB entry 3ke8; Gräwert *et al.*, 2010) catalyzes the final step of the nonmevalonate pathway for the biosynthesis of the terpene precursors isopentenyl diphosphate and dimethylallyl diphosphate. This reaction proceeds *via* reductive dehydration of 1-hydroxy-2-methyl-2-(*E*)-butenyl-4-diphosphate, and IspH requires a [4Fe–4S] cluster. Dph2 (PDB entry 3lzd; Zhang *et al.*, 2010) catalyzes the transfer of an aminopropyl group, derived from *S*-adenosylmethionine (SAM), to a histidine residue in the first step in the biosynthesis of diphthamide, a specific post-translational histidine modification found only in elongation factor 2. Dph2 also contains a [4Fe–4S] cluster and is a unique radical SAM enzyme.

A superposition of individual domains from PfQS, IspH and Dph2 (Fig. 7*a*) demonstrates a common topology containing four β-strands (labeled $\beta1$–$\beta4$) flanked on one side by two α-helices ($\alpha1$ and $\alpha2$) that are always present and on the other side by at least one of two α-helices ($\alpha3$ and $\alpha4$) (Fig. 7*b*). In both IspH and Dph2, the three domains show a triangular arrangement (Fig. 8). IspH and PhQS show threefold pseudosymmetry, while Dph2 does not. In IspH and Dph2, the [4Fe–4S] cluster is located in the center of the triangle and one coordinating cysteine residue comes from each of the three monomers (Fig. 7*b*). Comparison of the monomers shows some important differences. The domains of PfQS and IspH are generally oriented in the same way relative to the axis of threefold pseudosymmetry. The centers of PfQS domains 1, 2 and 3 fall roughly on the centers of IspH domains 1, 2 and 3, respectively. However, each of the domains of PfQS is tilted by about 30° with respect to the corresponding domain in IspH. In addition, the locations of the [4Fe–4S]-chelating cysteine residues show variation with respect to the domain topology. In PfQS, which lacks the [4Fe–4S] cluster, the cysteine residue of each domain is in a disordered loop following strand $\beta4$ (Fig. 7*b*). In IspH, the cysteine residues are all well ordered and are located in the loop preceding helix $\alpha1$. In the case of Dph2, domains 2 and 3 are rotated by approximately 180 and 90°, respectively, with respect to domain 1. In domains 1 and 2 the conserved cysteine residues are located in the loop between $\beta2$ and $\alpha3$, while the conserved cysteine residue of domain 3 is located in the loop between $\beta3$ and $\alpha4$.

4.6. A model for the QS active site with a [4Fe–4S] cluster

Attempts to crystallize reconstituted PfQS were unsuccessful. The structure of PhQS (PDB entry 1wzu) did not contain a [4Fe–4S] cluster, but contained the substrate analog malate (Sakuraba *et al.*, 2005). Furthermore, all three conserved cysteine residues in PhQS fell in disordered loops and were not included in the deposited PDB file. In PfQS two of the conserved cysteine residues are well ordered and most of the loop containing the third cysteine residue is present; however, PfQS is in the inactive dimeric form. By combining the two QS models, we were able to place the conserved cysteine residues in reasonable positions in the monomeric PhQS structure. We then used a superposition of IspH and PfQS to model the cysteine residues to position the [4Fe–4S] cluster, which required only slight manual adjustment.

The malate molecule from the PhQS crystal structure was used as a guide to position a model of

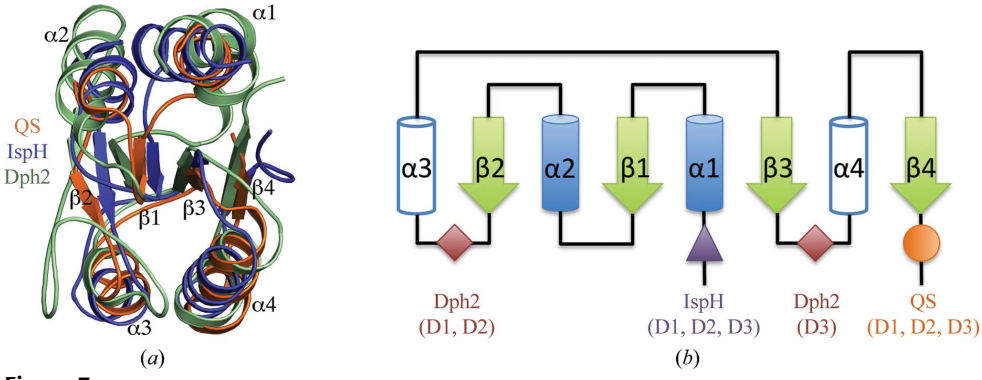

Figure 7
Comparison of the conserved domains of PfQS, IspH and Dph2. (*a*) Superposition of domain 2 from each enzyme. The color-coding is by protein and is indicated by the labels. The α-helices and β-strands are each numbered 1–4. (*b*) Topology of the common domain fold, showing the locations of the conserved cysteine residues. The four β-strands are found in all three domains of each protein. The blue α-helices ($\alpha1$ and $\alpha2$) are found in all three domains of all three proteins and at least one of the white α-helices ($\alpha3$ and $\alpha4$) is found in each domain of each protein. The locations of the conserved cysteine residues with respect to the domain topology are shown as a yellow circle for PfQS, as a purple triangle for IspH and as a pink square for Dph2.

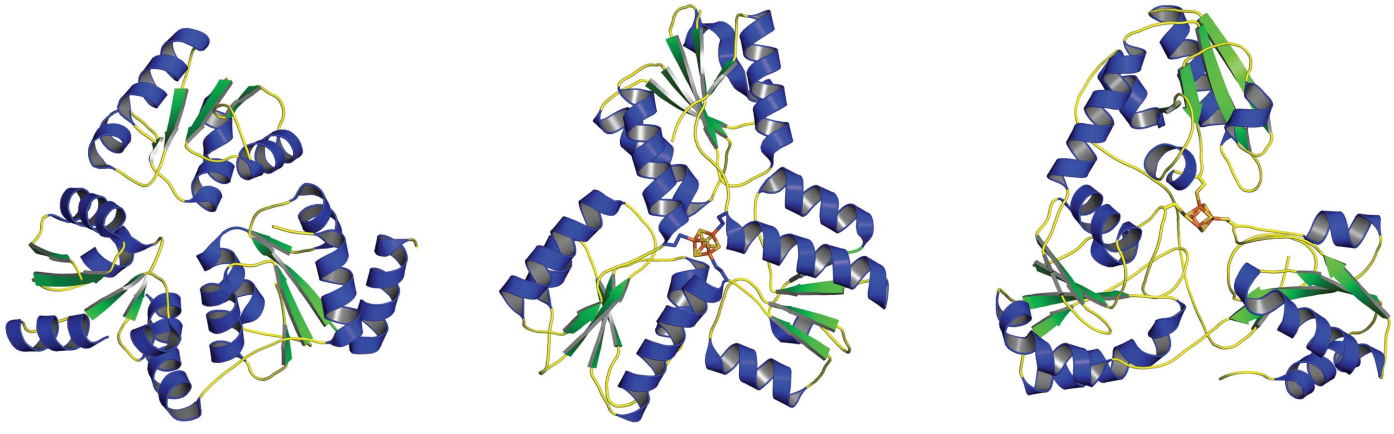

Figure 8
Comparison of the PhQS, IspH and Dph2 monomers. Color-coding is by secondary structure. The [4Fe–4S] clusters of IspH and Dph2 are shown as stick models. The proteins were oriented so that the active-site cavity is exposed and the domains are in relative positions.

the final intermediate, 5-hydroxy-4,5-dihydroquinolinate (Fig. 9*a*). The interactions with the carboxylate atoms were maintained and the ring was constructed using either *R* or *S* stereochemistry at C5. In the *R*-enantiomer the 5-hydroxyl group pointed towards the fourth Fe atom of the [4Fe–4S] cluster with a distance of about 3 Å. This model is consistent with the proposal that the [4Fe–4S] cluster facilitates a final dehydration leading to the production of quinolinate.

A model of the substrate complex with DHAP and iminoaspartate was also prepared (Fig. 9*b*). Iminoaspartate was generated by converting the 2-hydroxyl group of malate to an imino group and keeping the O atoms of the two carboxylate groups fixed in their experimentally determined positions. The resulting model showed a clear cavity between the [4Fe–4S] cluster and the iminoaspartate that is approximately the right size and shape to accommodate a molecule of DHAP. DHAP was oriented so that the atoms involved in the formation of the pyridine ring were close to each other. Namely, the amino group of iminoaspartate is near C1 of DHAP and C3 of iminoaspartate is near C3 of DHAP. In this orientation the phosphate group makes several hydrogen bonds, while if the direction of DHAP were reversed the phosphate would insert into a small hydrophobic cavity. Interestingly, to be consistent with the expected connectivity of the final intermediate, the direction of malate needed to be reversed. Examination of PDB entry 1wzu showed that the electron density for the ligand could be fitted equally well with either L-malate in the orientation shown by the authors or by D-malate with the carboxylate groups interchanged. The source of malate was not described in the original publication, nor was the malate enantiomer (Sakuraba *et al.*, 2005). Therefore, it is reasonable to conclude that the bound species is likely to be a 50:50 mixture of racemic malate.

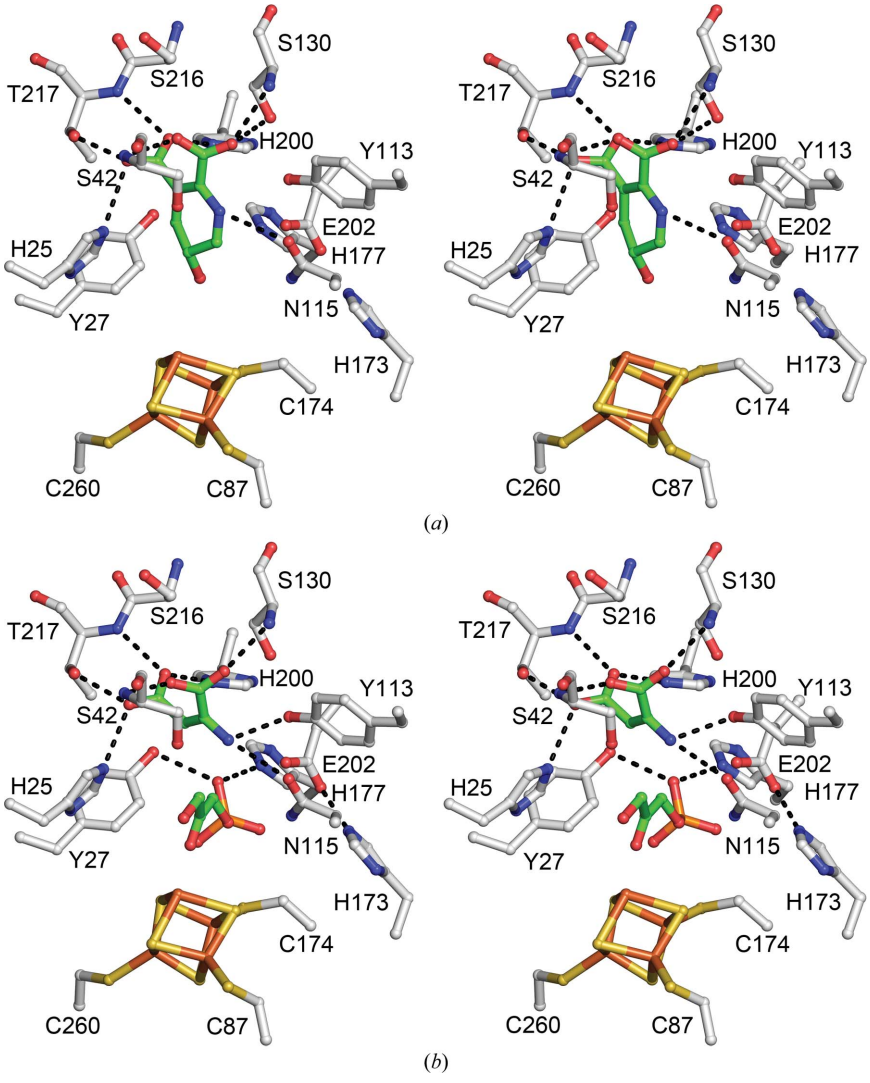

Figure 9
Ball-and-stick models of PfQS with a [4Fe–4S] cluster and ligands. (*a*) Complex with the final intermediate 5-hydroxy-4,5-dihydroquinolinate. (*b*) Enzyme–substrate complex with iminoaspartate and DHAP. C atoms are white for PfQS and green for the ligand. N atoms are blue, O atoms are red, S atoms are yellow and Fe atoms are orange. The residues shown are the three cysteine residues that anchor the [4Fe–4S] cluster and residues that make van der Waals contacts or hydrogen bonds with at least one atom of the ligand. Hydrogen bonds are indicated by dashed lines.

The resulting QS models (Fig. 9) contain a [4Fe–4S] cluster with Cys87, Cys174 and Cys260 ligated to three of the Fe atoms. The fourth Fe atom is oriented towards DHAP, which is located between the cluster and iminoaspartate, or the 5-hydroxy group of the intermediate. The model is consistent with a previous proposal by Booker and coworkers in which the [4Fe–4S] cluster serves as a Lewis acid for the final dehydration step (Cicchillo *et al.*, 2005). In addition, Ollagnier-de Choudens and coworkers recently used Mössbauer spectroscopy to show that the QS inhibitor 4,5-dithiohydroxyphthalic acid binds to a differentiated iron site of the [4Fe–4S] cluster (Chan *et al.*, 2012). In a model generated using density functional theory, both sulfhydryl groups coordinate to the differentiated iron site of the [4Fe–4S] cluster. In this model of the inhibitor complex, the plane of the aromatic ring bisects the [4Fe–4S] cluster, while in our model of the final reaction intermediate the six-membered ring has is rotated by approximately 90° on orientation.

All amino-acid residues shown in Fig. 9 are absolutely conserved in all QSs and our model is consistent with the expected substrate-binding geometry. Therefore, QS appears to be the third member of a structural family containing [4Fe–4S] clusters in which the cysteine residues are found in separate structural domains and the domains show a triangular arrangement, with the [4Fe–4S] cluster located in the center of the three domains. In IspH and QS the [4Fe–4S] cluster appears to serve as a

Lewis acid, while in the unusual radical SAM enzyme Dph2 the [4Fe–4S] cluster participates in the generation of an aminocarboxypropyl radical, suggesting that this [4Fe–4S]-cluster family of enzymes may be both more versatile and more widespread then previously recognized.

We thank the Northeastern Collaborative Access Team beamline 8-BM of the Advanced Photon Source, supported by award grant RR-15301 from the National Center for Research Resources at the National Institutes of Health, for beamtime. Use of the Advanced Photon Source is supported by the US Department of Energy, Office of Basic Energy Sciences under Contract No. DE-AC02-06CH11357. We thank Leslie Kinsland for assistance with this manuscript.

References

Adams, P. D., Grosse-Kunstleve, R. W., Hung, L.-W., Ioerger, T. R., McCoy, A. J., Moriarty, N. W., Read, R. J., Sacchettini, J. C., Sauter, N. K. & Terwilliger, T. C. (2002). *Acta Cryst.* D**58**, 1948–1954.
Ausubel, F. M. & Brent, F. (1987). *Current Protocols in Molecular Biology*. New York: John Wiley & Sons.
Bacchella, L., Lina, C., Todone, F., Negri, A., Tedeschi, G., Ronchi, S. & Mattevi, A. (1999). *Acta Cryst.* D**55**, 549–551.
Begley, T. P., Kinsland, C., Mehl, R. A., Osterman, A. & Dorrestein, P. (2001). *Vitam. Horm.* **61**, 103–119.
Berger, F., Ramírez-Hernández, M. H. & Ziegler, M. (2004). *Trends Biochem. Sci.* **29**, 111–118.
Björkman, A. J., Binnie, R. A., Zhang, H., Cole, L. B., Hermodson, M. A. & Mowbray, S. L. (1994). *J. Biol. Chem.* **269**, 30206–30211.
Bradford, M. M. (1976). *Anal. Biochem.* **72**, 248–254.
Brünger, A. T., Adams, P. D., Clore, G. M., DeLano, W. L., Gros, P., Grosse-Kunstleve, R. W., Jiang, J.-S., Kuszewski, J., Nilges, M., Pannu, N. S., Read, R. J., Rice, L. M., Simonson, T. & Warren, G. L. (1998). *Acta Cryst.* D**54**, 905–921.
Ceciliani, F., Caramori, T., Ronchi, S., Tedeschi, G., Mortarino, M. & Galizzi, A. (2000). *Protein Expr. Purif.* **18**, 64–70.
Chan, A., Clémancey, M., Mouesca, J.-M., Amara, P., Hamelin, O., Latour, J.-M. & Ollagnier de Choudens, S. (2012). *Angew. Chem. Int. Ed. Engl.* **51**, 7711–7714.
Chatterjee, A., Jurgenson, C. T., Schroeder, F. C., Ealick, S. E. & Begley, T. P. (2007). *J. Am. Chem. Soc.* **129**, 2914–2922.
Cicchillo, R. M., Tu, L., Stromberg, J. A., Hoffart, L. M., Krebs, C. & Booker, S. J. (2005). *J. Am. Chem. Soc.* **127**, 7310–7311.
DeLano, W. L. (2002). *PyMOL*. http://www.pymol.org.
Draczynska-Lusiak, B. & Brown, O. R. (1992). *Free Radic. Biol. Med.* **13**, 689–693.
Emsley, P. & Cowtan, K. (2004). *Acta Cryst.* D**60**, 2126–2132.
Esnouf, R. M. (1997). *J. Mol. Graph.* **15**, 132–134.
Esnouf, R. M. (1999). *Acta Cryst.* D**55**, 938–940.
Flachmann, R., Kunz, N., Seifert, J., Gütlich, M., Wientjes, F. J., Läufer, A. & Gassen, H. G. (1988). *Eur. J. Biochem.* **175**, 221–228.
Gardner, P. R. & Fridovich, I. (1991). *Arch. Biochem. Biophys.* **284**, 106–111.
Gräwert, T., Span, I., Eisenreich, W., Rohdich, F., Eppinger, J., Bacher, A. & Groll, M. (2010). *Proc. Natl Acad. Sci. USA*, **107**, 1077–1081.
Holm, L. & Sander, C. (1993). *J. Mol. Biol.* **233**, 123–138.
Jones, T. A., Zou, J.-Y., Cowan, S. W. & Kjeldgaard, M. (1991). *Acta Cryst.* A**47**, 110–119.
Kleywegt, G. J. & Jones, T. A. (1996). *Acta Cryst.* D**52**, 826–828.
Knight, J. R. & Milner, J. (2012). *Curr. Opin. Oncol.* **24**, 68–75.
Kurnasov, O., Goral, V., Colabroy, K., Gerdes, S., Anantha, S., Osterman, A. & Begley, T. P. (2003). *Chem. Biol.* **10**, 1195–1204.
Loiseau, L., Ollagnier-de Choudens, S., Lascoux, D., Forest, E., Fontecave, M. & Barras, F. (2005). *J. Biol. Chem.* **280**, 26760–26769.
Magni, G., Amici, A., Emanuelli, M., Raffaelli, N. & Ruggieri, S. (1999). *Adv. Enzymol. Relat. Areas Mol. Biol.* **73**, 135–182.
Marinoni, I., Nonnis, S., Monteferrante, C., Heathcote, P., Härtig, E., Böttger, L. H., Trautwein, A. X., Negri, A., Albertini, A. M. & Tedeschi, G. (2008). *FEBS J.* **275**, 5090–5107.
Matthews, B. W. (1968). *J. Mol. Biol.* **33**, 491–497.
Merritt, E. A. & Bacon, D. J. (1997). *Methods Enzymol.* **277**, 505–524.
Miller, R., DeTitta, G. T., Jones, R., Langs, D. A., Weeks, C. M. & Hauptman, H. A. (1993). *Science*, **259**, 1430–1433.
Miller, R., Gallo, S. M., Khalak, H. G. & Weeks, C. M. (1994). *J. Appl. Cryst.* **27**, 613–621.
Murshudov, G. N., Skubák, P., Lebedev, A. A., Pannu, N. S., Steiner, R. A., Nicholls, R. A., Winn, M. D., Long, F. & Vagin, A. A. (2011). *Acta Cryst.* D**67**, 355–367.
Narayana Murthy, U. M., Ollagnier-de-Choudens, S., Sanakis, Y., Abdel-Ghany, S. E., Rousset, C., Ye, H., Fontecave, M., Pilon-Smits, E. A. & Pilon, M. (2007). *J. Biol. Chem.* **282**, 18254–18264.
Nasu, S. & Gholson, R. K. (1981). *Biochem. Biophys. Res. Commun.* **101**, 533–539.
Nasu, S., Wicks, F. D. & Gholson, R. K. (1982). *J. Biol. Chem.* **257**, 626–632.
Ollagnier-de Choudens, S., Loiseau, L., Sanakis, Y., Barras, F. & Fontecave, M. (2005). *FEBS Lett.* **579**, 3737–3743.
Otwinowski, Z. & Minor, W. (1997). *Methods Enzymol.* **276**, 307–326.
Pollak, N., Dölle, C. & Ziegler, M. (2007). *Biochem. J.* **402**, 205–218.
Rousset, C., Fontecave, M. & Ollagnier de Choudens, S. (2008). *FEBS Lett.* **582**, 2937–2944.
Sakuraba, H., Tsuge, H., Yoneda, K., Katunuma, N. & Ohshima, T. (2005). *J. Biol. Chem.* **280**, 26645–26648.
Sambrook, J., Fritsch, E. F. & Maniatis, T. (1989). *Molecular Cloning: A Laboratory Manual*. Plainview: Cold Spring Harbor Laboratory Press.
Saunders, A. H. & Booker, S. J. (2008). *Biochemistry*, **47**, 8467–8469.
Saunders, A. H., Griffiths, A. E., Lee, K. H., Cicchillo, R. M., Tu, L., Stromberg, J. A., Krebs, C. & Booker, S. J. (2008). *Biochemistry*, **47**, 10999–11012.
Seifert, J., Kunz, N., Flachmann, R., Läufer, A., Jany, K. & Gassen, H. G. (1990). *Biol. Chem. Hoppe Seyler*, **371**, 239–248.
Sun, D. & Setlow, P. (1993). *J. Bacteriol.* **175**, 1423–1432.
Suzuki, N., Carlson, J., Griffith, G. & Gholson, R. K. (1973). *Biochim. Biophys. Acta*, **304**, 309–315.
Thompson, J. D., Higgins, D. G. & Gibson, T. J. (1994). *Nucleic Acids Res.* **22**, 4673–4680.
Wicks, F. D., Sakakibara, S. & Gholson, R. K. (1978). *J. Bacteriol.* **136**, 136–141.
Wicks, F. D., Sakakibara, S., Gholson, R. K. & Scott, T. A. (1977). *Biochim. Biophys. Acta*, **500**, 213–216.
Zhang, Y., Zhu, X., Torelli, A. T., Lee, M., Dzikovski, B., Koralewski, R. M., Wang, E., Freed, J., Krebs, C., Ealick, S. E. & Lin, H. (2010). *Nature (London)*, **465**, 891–896.